

Ca II and Na I absorption signatures from extraplanar gas in the halo of the Milky Way^{*}

N. Ben Bekhti¹, P. Richter², T. Westmeier³, and M. T. Murphy⁴

¹ Argelander-Institut für Astronomie, Universität Bonn, Auf dem Hügel 71, 53121 Bonn, Germany
e-mail: nbekhti@astro.uni-bonn.de

² Institut für Physik und Astronomie, Universität Potsdam, Haus 28, Karl-Liebknecht-Str. 24/25, 14476 Potsdam, Germany
e-mail: prichter@astro.physik.uni-potsdam.de

³ Australia Telescope National Facility, PO Box 76, Epping NSW 1710, Australia
e-mail: tobias.westmeier@csiro.au

⁴ Centre for Astrophysics & Supercomputing, Swinburne University of Technology, Hawthorn, Victoria 3122, Australia
e-mail: mmurphy@swin.edu.au

Received 14 November 2007 / Accepted 11 June 2008

ABSTRACT

Aims. We analyse absorption characteristics and physical conditions of extraplanar intermediate- and high-velocity gas to study the distribution of the neutral and weakly ionised Milky Way halo gas and its relevance for the evolution of the Milky Way and other spiral galaxies.

Methods. We combine optical absorption line measurements of Ca II/Na I and 21 cm emission line observations of HI along 103 extragalactic lines of sight towards quasars (QSOs) and active galactic nuclei (AGN). The archival optical spectra were obtained with the Ultraviolet and Visual Echelle Spectrograph (UVES) at the ESO Very Large Telescope, while the 21 cm HI observations were carried out using the 100-m radio telescope at Effelsberg.

Results. The analysis of the UVES spectra shows that single and multi-component Ca II/Na I absorbers at intermediate and high velocities are present in about 35 percent of the sight lines, indicating the presence of neutral extraplanar gas structures. In some cases the Ca II/Na I absorption is connected with HI 21 cm intermediate- or high-velocity gas with HI column densities in the range of 10^{18} to 10^{20} cm⁻² (i.e., the classical IVCs and HVCs), while other Ca II/Na I absorbers show no associated HI emission. The observed HI line widths vary from $\Delta v_{FWHM} = 3.2$ km s⁻¹ to 32.0 km s⁻¹ indicating a range of upper gas temperature limits of 250 K up to about 22 500 K.

Conclusions. Our study suggests that the Milky Way halo is filled with a large number of neutral gaseous structures whose high column density tail represents the population of common HI high-velocity clouds seen in 21 cm surveys. The Ca II column density distribution follows a power-law $f(N) = CN^\beta$ with a slope of $\beta \approx -1.6$, thus comparable to the distribution found for intervening metal-line systems toward QSOs. Many of the statistical and physical properties of the Ca II absorbers resemble those of strong ($W_{\lambda 2796} > 0.3$ Å) Mg II absorbing systems observed in the circumgalactic environment of other galaxies, suggesting that both absorber populations may be closely related.

Key words. Galaxy: halo – ISM: structure – quasars: absorption lines – galaxies: halo

1. Introduction

Spiral galaxies are surrounded by large gaseous halos. That the disk of the Milky Way has a hot envelope was first proposed by Spitzer (1956). Spitzer considered such a “Galactic Corona” to explain spectroscopic observations that have been made earlier by Adams (1949) and Münch (1952). In recent years, great instrumental progress has been made to measure extraplanar gas structures around other galaxies, as well. It became clear, that the gaseous halos represent the interface between the condensed galactic discs and the surrounding intergalactic medium (IGM) (e.g., Savage & Massa 1987; Majewski 2004; Fraternali et al. 2007, and references therein). The properties of this medium around galaxies presumably are determined by both, the accretion of metal-poor gaseous matter from intergalactic space onto the galactic disc, as well as the outflow of metal-enriched gas caused by star formation activity within the galaxy (e.g.,

Sembach et al. 2003a; Fraternali & Binney 2006, and references therein).

Gas in the halos and intergalactic environment of galaxies leaves its imprint in the spectra of distant quasars (QSOs) in the form of hydrogen- and metal-line absorption (for a recent review, see Richter 2006). Therefore, QSO absorption spectroscopy has become a powerful method to study the physical properties, the kinematics, and the spatial distribution of gas in the halos of galaxies over a large range of column densities at low and high redshifts. The analysis of intervening Mg II and C IV absorption line systems (e.g., Charlton et al. 2000; Ding et al. 2003a; Masiero et al. 2005; Bouché et al. 2006) and their relation to galactic structures suggest rather complex absorption characteristics of these ions indicating the multi-phase nature of gas in the outskirts of galaxies with density and temperature ranges spanning several order of magnitudes. Stronger intervening low-ion absorbers (e.g., strong Mg II systems) preferentially arise at low impact parameters ($< 35 h^{-1}$ kpc) of intervening galaxies, while weaker Mg II systems and high-ion absorbers (e.g.,

^{*} Figures 9 to 16 are only available in electronic form at <http://www.aanda.org>

C IV systems) apparently are often located at larger distances up to $\sim 100 h^{-1}$ kpc (Churchill et al. 1999; Milutinovic et al. 2006). Due to the lack of additional information the exact nature and origin of the various circumgalactic absorber populations is not yet fully understood. Most likely, gas outflow and infall processes both contribute to the complex absorption pattern observed.

Our own Galaxy also is surrounded by large amounts of neutral and ionised gas (Richter 2006). Most prominent are the so-called intermediate- and high-velocity clouds (IVCs, HVCs, Muller et al. 1963) which represent clouds of neutral atomic hydrogen seen in 21 cm emission at radial velocities inconsistent with a simple model of Galactic disk rotation. Most important for our understanding of the nature of IVCs and HVCs and their role for the evolution of the Milky Way is the determination of accurate metal abundances and distances of these clouds. Metallicity measurements are particularly important to learn about the origin of IVCs/HVCs. The metal abundances of some IVCs/HVCs have been determined by absorption line measurements along several lines of sight (see Wakker 2001; Richter 2006). The results show that the metallicities are varying between ~ 0.1 and ~ 1.0 solar. This wide range of metallicities suggests that many IVCs and HVCs cannot have a common origin. In fact, it is now widely accepted that various different processes contribute to the neutral gas flow in the Milky Way halo including the Galactic fountain (Shapiro & Field 1976; Bregman 1980; Shapiro & Benjamin 1991), the accretion of gas from surrounding satellite galaxies (e.g., Magellanic Stream, Mathewson et al. 1974), and the infall of metal-poor gas from the intergalactic medium (e.g., Wakker et al. 1999).

To determine the total mass of the gas that is falling toward the Milky Way disk in form of IVCs and HVCs a reliable distance estimate of these clouds is required. Measuring the distances of IVCs/HVCs is very difficult, however. The most reliable method to infer a distance bracket requires high-resolution spectra of stars with known distances in which IVCs/HVCs appear in absorption. The problem is the limited number of suitable background stars. The distance estimates of IVCs and HVCs around the Milky Way (e.g., Sembach et al. 1991; van Woerden et al. 1999; Wakker 2001; Thom et al. 2006; Wakker et al. 2007, 2008) indicate that most IVCs are relatively nearby objects with distances of $d < 2$ kpc while the majority of the HVCs are more distant clouds, located in the halo of the Milky Way with distances of $5 < d < 50$ kpc. These numbers imply that the typical mass-accretion rate from IVCs and HVC are on the order of one solar mass per year.

While there are a large number of recent absorption studies on the nature of IVCs and HVCs and their role for the evolution of the Milky Way, relatively little effort has been made to investigate the connection between the Galactic population of IVCs and HVCs and the distribution and nature of intervening metal-absorption systems from galaxy halos seen in QSO spectra. In fact, almost all recent absorption studies of IVCs and HVCs were carried out in the FUV to study in detail metal abundances and ionisation conditions of halo clouds using the many available transitions of low and high ions in the ultraviolet regime (e.g., Richter et al. 2001). These studies were designed as follow-up absorption observations of known IVCs and HVCs, thus providing an 21 cm *emission-selected* data set. However, to statistically compare the absorption characteristics of the extraplanar Galactic halo structures with the properties of intervening metal-absorption systems towards QSOs one requires an *absorption-selected* data set of IVCs and HVCs. Since in the UV band there are currently only a very limited number (<50) of high-quality

spectra available such a statistical comparison can be done best in the optical regime where a large number of high-quality spectra of low- and high-redshift QSOs are available.

In this paper we discuss low-column density extraplanar structures which are most likely located in the environment of the Milky Way detected in optical Ca II and Na I absorption towards quasars along 103 sight lines through the Milky Way halo. Our study allows us to directly compare the observed absorption column-density distribution of gas in the Milky Way halo with the overall column-density distribution of intervening metal absorbers toward QSOs and AGN. Moreover, our study enables us to identify neutral and ionised absorption structures at low gas column densities and small angular extent that remain unseen in the large 21 cm IVC and HVC all-sky surveys but that possibly have a considerable absorption cross section (see Richter et al. 2005). We supplement our absorption-line data with new HI 21 cm observations to investigate the relation between intermediate- and high-velocity Ca II absorption features and halo 21 cm emission. The study presented here discusses the first results of our analysis of the physical and statistical properties of the detected absorption and emission features. Additional absorption-line observations as well as follow-up HI synthesis observations of some of the absorbers are under way and will be presented in a subsequent paper (Ben Bekhti et al. 2008, in preparation).

Our paper is organised as follows. In Sect. 2 we describe the data acquisition and data reduction. In Sect. 3 the results of the analysis of the UVES and the Effelsberg data of 103 sight lines in the direction of several quasars are presented. A statistical investigation (column density distribution functions, distribution of b -values, deviation velocities, etc.) of the data is presented in Sect. 4. In Sect. 5 we discuss the results regarding multiple absorption lines and corresponding emission line measurements, the determination of metallicities and a probable association of the gas with known IVC and HVC complexes. In Sect. 6 we summarise our results and discuss future observations that will be required to determine the metallicities of the gas, important to understand the nature and origin of these intermediate- and high-velocity absorption features.

2. Data acquisition and reduction

2.1. UVES data

The data basis of our analysis are 103 optical spectra of high-redshift QSOs and AGN obtained with the Ultraviolet and Visual Echelle Spectrograph (UVES) between 1999 and 2004 at the ESO Very Large Telescope. These spectra, observed for various purposes by various groups, are publically available in the ESO data archive¹. The spectra used in this study have a spectral resolution of $R \approx 40\,000$ – $60\,000$, corresponding to approximately 6.6 km s^{-1} FWHM. For the normalised spectra the signal-to-noise ratio per resolution element

$$S/N_r = \sqrt{\frac{\Delta\lambda_r}{\Delta\lambda_p} \frac{1}{\sigma_p^{\text{rms}}}} \quad (1)$$

at the two Ca II lines near 4000 \AA is between 10 and 190 with a typical value (median) of about 90. The quantity $\Delta\lambda_{r,p}$ are the wavelength separations per resolution and pixel element, respectively. The noise per pixel is given by σ_p^{rms} . A detailed description of the UVES instrument is given by Dekker et al. (2000).

¹ <http://archive.eso.org/wdb/wdb/eso/uves/form>

Part of the raw data were reduced with the UVES pipeline implemented in the ESO-MIDAS software-package as part of the data reduction process of the UVES Large Programme (Bergeron et al. 2004). The pipeline reduction includes flat-fielding, bias- and sky-subtraction, and a relative wavelength calibration. The data were then normalised by a continuum fit using high-order polynomials. The remaining data were reduced and normalised as part of the UVES Spectral Quasar Absorption Database (SQUAD). A version of the UVES pipeline, modified to improve the flux extraction and wavelength calibration, was used to extract the echelle orders. These were combined using the custom-written code, UVESOPLER,² with inverse-variance weighting and a cosmic ray rejection algorithm, to form a single spectrum with a dispersion of $2.5 \text{ km s}^{-1} \text{ pixel}^{-1}$.

As the two Ca II lines at 3934.77 \AA and 3969.59 \AA represent a doublet, we define a detection limit for the high-velocity Ca II absorption of 4σ for the stronger line at $\lambda = 3934.77 \text{ \AA}$ and a 2σ limit for the weaker line at $\lambda = 3969.59 \text{ \AA}$. For the median (minimal, maximal) S/N_r of about 90 (10, 190) the former limit corresponds to an equivalent width limit of $W_\lambda \approx 4 \text{ m\AA}$ (50 m\AA , 2 m\AA). These limits can be converted to column density detection limits on the linear part of the curve of growth using

$$N = \frac{W_\lambda m_e c^2}{\pi e^2 \lambda^2 f}. \quad (2)$$

The spectral features were analysed via Voigt-profile fitting using the FITLYMAN package in MIDAS, which, among other parameters, delivers column densities and Doppler parameters (b -values).

2.2. Effelsberg data

The follow-up HI 21 cm observations were obtained in 2006 with the 100-m radio telescope at Effelsberg for which at 21 cm wavelength the half-power beam width (HPBW) is $9'$. For our observations, the velocity resolution is about 0.5 km s^{-1} , and the rms is a few times 10^{-2} K , while the integration time per sight line was about 25 min. The spectra were analysed using the GILDAS tool CLASS. In all spectra polynomial baselines of up to 4th order were fitted. For this purpose, windows were set individually around the line emission. All data within these windows were not considered for the fit. After the baseline fit Gaussian functions were fitted to the spectral lines.

2.3. The Leiden/Argentine/Bonn survey (LAB)

In addition to our Effelsberg observations we used archival data from the Leiden-Argentine-Bonn (LAB) all-sky HI 21 cm survey (Kalberla et al. 2005) for those sight lines where we do not have Effelsberg spectra to search for HI emission related to the optical absorption.

The LAB survey is a combination of the Leiden/Dwingeloo Survey (LDS, Hartmann & Burton 1997), covering the sky north of $\delta = -30^\circ$, and the Instituto Argentino de Radioastronomía Survey (IAR, Arnal et al. 2000; Bajaja et al. 2005) which covers the sky south of $\delta = -25^\circ$. The HPBW of the LAB survey is about $36'$. The LSR velocity coverage is in the range of -450 km s^{-1} to $+400 \text{ km s}^{-1}$, at a velocity resolution of 1.3 km s^{-1} . The entire LAB data was corrected for stray radiation at the Argelander-Institut für Astronomie in Bonn.

² Available at http://www.ast.cam.ac.uk/~mim/UVES_popler.html

3. Observational results and sample selection

Figure 1 shows an all-sky HVC map which was created by Westmeier (2007) based on the data of the LAB survey (Kalberla et al. 2005). On the one hand, several extended HI HVC complexes cover the sky (Wakker 1991), some of which are spanning tens of degrees. On the other hand, numerous isolated and compact HVCs can be seen all over the sky (Braun & Burton 1999; Putman et al. 2002; de Heij et al. 2002). However, most of these structures are not resolved with the $36'$ beam of the LAB survey. The symbols in Fig. 1 mark the positions of the 103 sight lines that were observed with UVES.

For the further analysis we have transformed all spectra to the Local Standard of Rest (LSR) velocity scale. Note most of the gas near zero velocities is located in the Galactic disk. To separate low-velocity gas in the disk from extraplanar intermediate- and high-velocity gas in the halo we have used the concept of the so-called deviation velocity together with a kinematic model for the Milky Way developed by Kalberla (2003). With this model we can determine whether an observed velocity in a given direction is expected for interstellar gas participating in the Galactic disk rotation or not. According to Wakker (1991) the deviation velocity is defined by

$$v_{\text{dev}} = \begin{cases} v_{\text{LSR}} - v_{\text{min}} & \text{if } v_{\text{LSR}} < 0 \\ v_{\text{LSR}} - v_{\text{max}} & \text{if } v_{\text{LSR}} > 0 \end{cases}, \quad (3)$$

where v_{min} and v_{max} are given by the rotation model of Kalberla (2003). We consider all absorption lines with $v_{\text{dev}} > 0$ (if $v_{\text{LSR}} > 0$) or $v_{\text{dev}} < 0$ (if $v_{\text{LSR}} < 0$) as intermediate- or high-velocity gas. To distinguish between IVCs and HVCs we use the definition of Wakker (1991) in which a cloud is defined as an IVC, if $|v_{\text{dev}}| \leq 50 \text{ km s}^{-1}$ and as an HVC if $|v_{\text{dev}}| > 50 \text{ km s}^{-1}$. Using these selection criteria for the 103 UVES spectra we detect 55 Ca II and 20 Na I halo absorption components along 35 lines of sight at intermediate and high velocities. These 35 sightlines are indicated in Fig. 1 with the filled symbols. For 19 of these sight lines we have carried out deep HI 21 cm observations with the Effelsberg 100-m telescope to search for neutral hydrogen structures that are associated with the absorption systems.

A complete presentation of the 35 obtained spectra with optical absorption of Ca II $\lambda 3934.77 \text{ \AA}$, Ca II $\lambda 3969.59 \text{ \AA}$, Na I $\lambda 5891.58 \text{ \AA}$, Na I $\lambda 5897.56 \text{ \AA}$ together with the corresponding HI $\lambda 21 \text{ cm}$ emission profiles observed with the 100-m telescope at Effelsberg is given in the Appendix.

Some of the halo Ca II and Na I absorbers show multiple intermediate- and high-velocity components, indicating the presence of gaseous sub-structures. Furthermore, along 13 sight lines the intermediate- and high-velocity Ca II and Na I absorption is connected with HI gas with typical column densities in the range of a few times 10^{18} cm^{-2} up to 10^{20} cm^{-2} . The measured HI line widths vary from $\Delta v_{\text{FWHM}} = 3.2 \text{ km s}^{-1}$ to 32.0 km s^{-1} giving a range of upper gas temperature limits of 250 K up to about 22500 K . Measured column densities (UVES and Effelsberg) and b -values for the 35 sight lines are summarised in Tables 1 and 2.

It is important to note at this point that in many cases there is no high- or intermediate-velocity HI 21 cm emission seen in the low-resolution LAB survey, whereas the higher resolution Effelsberg telescope detects emission lines at the corresponding position. This demonstrates how important high-resolution measurements are in view of beam smearing effects and the fact that the HI column densities of most of the Ca II and Na I absorption components are close to or below the detection limit of

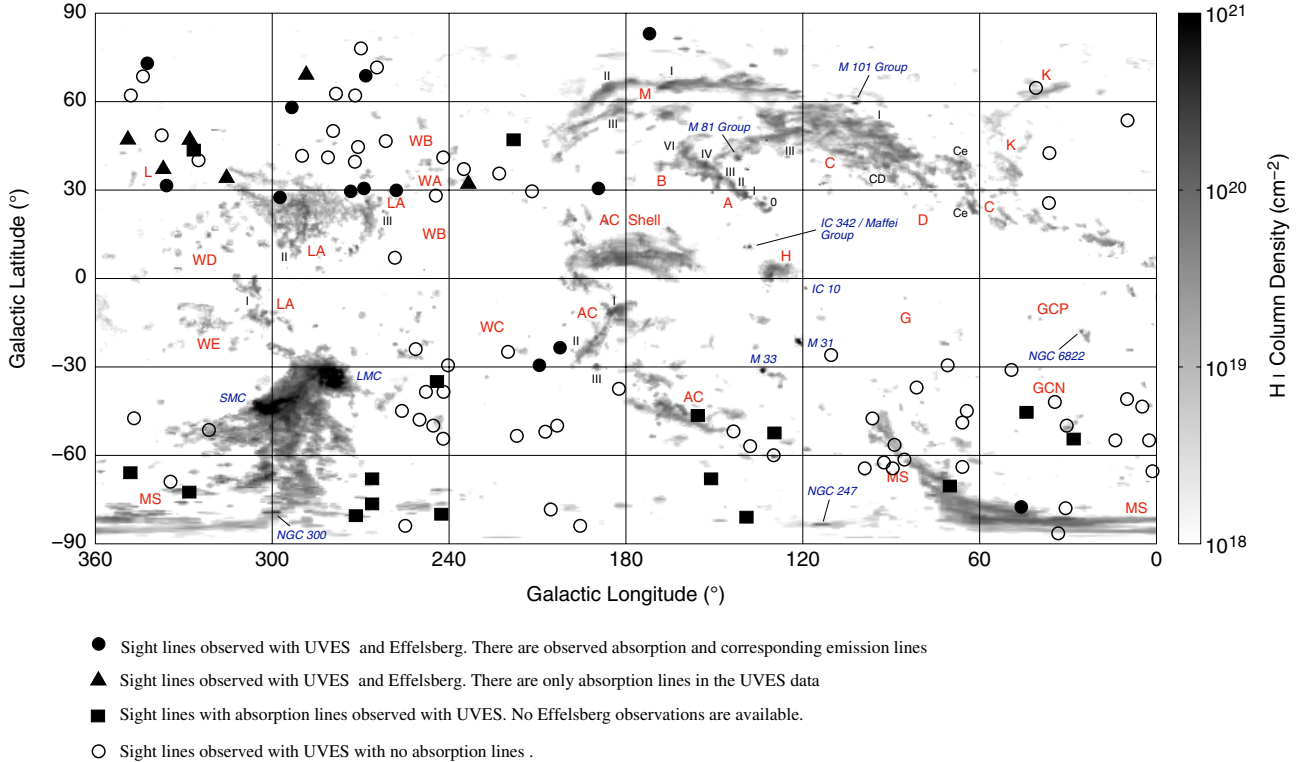


Fig. 1. HVC-all-sky map created by Westmeier (2007) derived from the data of the LAB Survey (Kalberla et al. 2005). The different symbols mark the positions of 103 sight lines that were observed with UVES. Along 35 lines of sight we detect Ca II/Na I absorption components. For 19 of them we have obtained additional H I observations with the Effelsberg 100-m telescope.

large H I surveys. One sight line (PKS 1448–232) with particularly prominent high-velocity Ca II and Na I absorption lines was observed by Richter et al. (2005) with UVES, Effelsberg, and the VLA. The high-resolution VLA H I data resolves the HVC into several compact, cold clumps. In our sample, 19 sight lines show intermediate- or high-velocity Ca II/Na I absorption without any corresponding counterparts in the H I data, suggesting that either the H I column densities are below the detection limit of the Effelsberg radio telescope or that the diameters of these clouds are very small so that beam-smearing effects make them undetectable.

The directions of several of the intermediate- and high-velocity absorbing systems as well as their velocities indicate a possible association with known large and extended HVC or IVC complexes, independent of whether they are detected in 21 cm or not. Other sight lines, in contrast, do not appear to be associated with any known HVC or IVC complex. Obviously, optical absorption spectra allow us to trace the low neutral column density environment of the Galactic halo. The distribution of neutral or weakly ionised gas is more complex than indicated by H I 21 cm observations alone.

Although the column densities have been measured with high accuracy, observations with high-resolution synthesis telescopes would be required to determine reliable Ca or Na abundances of the intermediate- and high-velocity gas. Another difficulty of Ca and Na measurements are the complex ionisation properties of calcium and sodium as well as dust depletion effects which introduce uncertainties in elemental abundance studies of these species (see Wakker & Mathis 2000). Note, that ionised material may represent a significant if not dominant fraction of the total gas amount of these gaseous material. The ionisation stage and the depletion of an element depends on the physical conditions in the halo, which may vary from location

to location (Sembach & Savage 1996). Another critical aspect is that many of the sight lines have blending problems with high-redshift ($z > 2$) Ly α forest lines. The consequence is that a significant fraction of Ca II and Na I high-velocity features may even remain unnoticed.

4. Statistical properties

We performed a statistical analysis of the 55 Ca II and 20 Na I intermediate and high velocity absorption components detected along 35 sight lines. In the following we turn our attention only to the Ca II absorption lines because there are only a few Na I absorption components compared to a large number of Ca II detections.

4.1. Column densities

Figure 2 shows the Ca II column density distribution (CDD) function, $f(N)$, derived from the UVES data. Following Churchill et al. (2003), we define

$$f(N) = \frac{m}{\Delta N}, \quad (4)$$

where m is the number of clouds in the column density range $[N, N + \Delta N]$. Integrating $f(N)$ over the observed column density range yields the total number of clouds, M , as

$$M = \int_{N_{\min}}^{N_{\max}} dN f(N). \quad (5)$$

The distribution of the Ca II column densities for $\log N_{\text{CaII}} > 11.6$ follows a power law $f(N) = CN^\beta$ with $\beta = -1.6 \pm 0.3$

Table 1. Summary of the UVES and Effelsberg measurements for intermediate and high velocity Ca II and Na I absorbers toward 20 quasars. The columns give the name of the quasars, the coordinates, the velocities in the LSR frame, the logarithm of the Ca II column densities, the b -value for the Ca II lines, the logarithm of the Na I column densities, the b -value for the Na I lines, the HI column densities, the b -value for the HI lines and the possibly associated HVC/IVC complex. The 4σ and 2σ detection limit (Sect. 2) for Ca II $\lambda 3934.77$ and Ca II $\lambda 3969.59$, respectively, corresponds to a $\log(N_{\text{CaII}}/\text{cm}^{-2})$ detection limit of ≈ 11 . n/a means that no Effelsberg data are available for these sight lines.

Quasar	l	b	v_{LSR}	$\log N_{\text{CaII}}$	b_{CaII}	$\log N_{\text{NaI}}$	b_{NaI}	$\log N_{\text{HI}}$	b_{HI}	HVC/IVC
	[$^{\circ}$]	[$^{\circ}$]	[km s^{-1}]	[N in cm^{-2}]	[km s^{-1}]	[N in cm^{-2}]	[km s^{-1}]	[N in cm^{-2}]	[km s^{-1}]	complex
QSO J1232-0224	293.2	60.1	-21	11.5	2	11.0	1	19.9	10.2	–
QSO B1101-26	275.0	30.2	199	11.7	6	–	–	–	–	LA
			-17	11.7	6	11.2	3	20.1	6.8	–
			-27	11.3	4	–	–	–	–	–
QSO J0003-2323	49.4	-78.6	-98	11.9	6	–	–	–	–	MS
			-112	11.8	6	–	–	19.6	19.3	MS
			-126	11.9	6	–	–	–	–	MS
QSO B0450-1310B	211.8	-32.1	-5	–	–	11.5	5	19.8	2.3	–
			-20	–	–	12.0	2	19.3	6.8	–
QSO B0515-4414	249.6	-35.0	-5	11.7	3	9.4	2	n/a	–	–
			-17	10.9	1	–	–	n/a	–	–
			-41	11.3	4	10.8	3	n/a	–	–
			-58	11.3	1	–	–	n/a	–	–
QSO B1036-2257	267.4	30.4	-24	11.9	7	12.0	1	19.6	2.0	–
QSO J1344-1035	323.5	50.2	-65	11.8	4	–	–	–	–	–
QSO B0109-353	275.5	-81.0	79	12.4	7	11.0	6	n/a	–	–
			-108	12.4	7	–	–	n/a	–	MS
			-162	12.3	12	–	–	n/a	–	MS
QSO B1448-232	335.4	31.7	-100	10.9	2	–	–	–	–	L
			-130	11.6	9	–	–	–	–	L
			-150	11.6	1	11.8	2	18.9	5.2	L
			-157	11.5	5	–	–	–	–	L
QSO B0002-422	332.7	-72.4	89	11.8	6	–	–	n/a	–	MS
QSO B0122-379	271.9	-77.3	40	11.7	4	–	–	n/a	–	MS
QSO B1347-2457	319.5	35.8	-95	11.5	3	–	–	–	–	–
J092913-021446	235.7	33.2	176	11.7	3	–	–	–	–	WA
J081331+254503	196.9	28.6	-23	–	–	11.1	5	19.8	37.0	–
J222756-224302	32.6	-57.3	-118	12.1	7	–	–	n/a	–	–
QSO J0830+2411	200.0	31.9	-21	–	–	11.3	3	19.2	7.6	–
QSO B0952+179	216.5	48.4	-30	–	–	11.6	9	n/a	–	IV Spur
QSO J2155-0922	47.5	-44.8	-166	11.1	1	–	–	n/a	–	GCN
			-209	11.8	6	–	–	n/a	–	GCN
QSO J1211+1030	271.7	70.9	76	11.5	2	–	–	–	–	–
			-26	11.6	4	–	–	19.7	13.5	IV Spur?
J143649.8-161341	336.6	39.7	76	11.4	3	–	–	–	–	–

and $\log C = 8.0 \pm 3.1$. The vertical and horizontal errorbars indicate Poisson and statistical (from Voigt profile-fitting) errors, respectively. The vertical solid line indicates the UVES 4σ detection limit $\log(N_{\text{CaII}}/\text{cm}^{-2}) = 10.7$ for the median S/N_r and the dotted line represents the maximal detection limit $\log(N_{\text{CaII}}^{\text{max}}/\text{cm}^{-2}) = 11.7$ for the minimal S/N_r . The minimal detection limit $\log(N_{\text{CaII}}^{\text{min}}/\text{cm}^{-2}) = 10.4$ for the maximal S/N_r is not plotted in Fig. 2. Note, that only the statistical noise is taken into account. The flattening of the distribution towards lower column densities therefore is caused by selection effects and other systematic errors (e.g., blending effects).

To better understand the relation between absorption-selected IVCs and HVCs from UVES and the 21 cm halo clouds seen with Effelsberg it would be very interesting to compare the column density distributions of these two data sets. It is known that Ca II qualitatively traces neutral gas in the interstellar medium (ISM). However, since Ca II is not the dominant ionisation stage of calcium in the diffuse ISM and calcium is depleted into dust grains the conversion between Ca II column densities and HI column densities is afflicted with large

systematic uncertainties and thus has to be used with caution. Yet, it is an observational fact that there exists such relation between the column densities of these two ions in the ISM as shown by (Wakker & Mathis 2000). These authors find a correlation between the abundance $A(\text{Ca II})$ and N_{HI} from 21 cm data in the form

$$\log(N_{\text{HI}}/\text{cm}^{-2}) = \frac{\log(N_{\text{CaII}}/\text{cm}^{-2}) - 7.45}{0.22}. \quad (6)$$

Although the scatter in this relation is substantial (see Wakker & Mathis 2000, their Fig. 1) Eq. (5) allows us to roughly estimate HI column densities from our measured Ca II column densities and to compare the column density distributions from absorption and emission. Note that at the current state we are not able to calculate a relation between Ca II and HI from our 21 cm data as we would have only ten data points available.

Figure 3 shows the converted HI column density distribution function $f(N)$. The dashed line represents a power law fit $f(N) = CN^{\beta}$, with $\beta = -1.3 \pm 0.1$ and $\log C = 7.4 \pm 2.3$ defined over the range of column densities from $\log(N_{\text{HI}}/\text{cm}^{-2}) = 19.5$

Table 2. Summary of the UVES and Effelsberg measurements for intermediate and high velocity Ca II and Na I absorbers toward 15 quasars. The columns give the name of the quasars, the coordinates, the velocities in the LSR frame, the logarithm of the Ca II column densities, the b -value for the Ca II lines, the logarithm of the Na I column densities, the b -value for the Na I lines, the HI column densities, the b -value for the HI lines and the possibly associated HVC/IVC complex. The 4σ and 2σ detection limit (Sect. 2) for Ca II $\lambda 3934.77$ and Ca II $\lambda 3969.59$, respectively, corresponds to a $\log(N_{\text{CaII}}/\text{cm}^{-2})$ detection limit of ≈ 11 . n/a means that no Effelsberg data are available for these sight lines.

Quasar	l	b	v_{LSR}	$\log N_{\text{CaII}}$	b_{CaII}	$\log N_{\text{NaI}}$	b_{NaI}	$\log N_{\text{HI}}$	b_{HI}	HVC/IVC
	[°]	[°]	[km s ⁻¹]	[N in cm ⁻²]	[km s ⁻¹]	[N in cm ⁻²]	[km s ⁻¹]	[N in cm ⁻²]	[km s ⁻¹]	complex
QSO B1212+3326	173.1	80.1	-37	11.0	4	11.0	2	-	-	IV Arch?
			-49	11.5	2	10.5	2	19.7	18.1	IV Arch?
			-57	11.6	8	-	-	-	-	IV Arch?
			-76	11.0	4	-	-	-	-	IV Arch?
QSO J1039-2719	270.0	27.0	184	11.3	5	-	-	-	-	WD
			-11	12.6	1	11.6	6	20.1	6.8	-
J123437-075843	290.4	70.4	88	11.6	2	-	-	-	-	-
			74	11.9	7	-	-	-	-	-
QSO B1331+170	348.5	75.8	-9	12.4	11	11.3	6	18.9	2.7	-
			-27	12.0	5	11.3	3	-	-	IV Spur
J144653+011355	354.7	52.1	16	11.8	4	-	-	-	-	-
			-48	11.5	4	-	-	-	-	-
QSO B2314-409	352.0	-66.3	-37	12.1	7	-	-	n/a	-	IV Spur
			-56	11.9	5	-	-	n/a	-	IV Spur
QSO J1356-1101	327.7	48.7	-108	12.0	6	-	-	n/a	-	-
QSO B0458-0203	201.5	-25.3	-7	12.1	4	12.1	2	19.3	2.6	AC shell
QSO J0103+1316	127.3	-49.5	-351	11.7	4	-	-	n/a	-	-
QSO J0153-4311	268.9	-69.6	124	12.4	6	-	-	n/a	-	MS
QSO B0216+0803	156.9	-48.7	11	12.1	1	-	-	n/a	-	-
QSO B2348-147	72.1	-71.2	91	11.4	1	-	-	n/a	-	MS
QSO J0139-0824	156.2	-68.2	-100	12.2	2	-	-	n/a	-	MS
QSO B0112-30	245.5	-84.0	-13	11.9	2	13.1	1	n/a	-	-
QSO J0105-1846	144.5	-81.1	192	11.4	1	-	-	n/a	-	MS
			167	11.2	3	-	-	n/a	-	MS
			108	11.4	2	11.0	3	n/a	-	MS

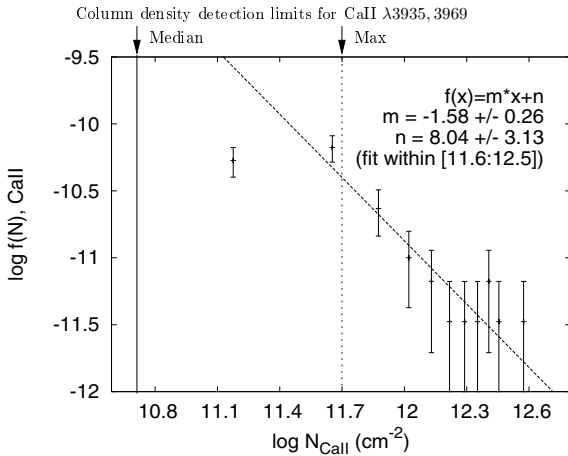


Fig. 2. The Ca II column density distribution $f(N)$ derived from UVES data. The dashed line represents a power-law fit $f(N) = CN^\beta$ with $\beta = -1.6 \pm 0.3$ and $\log C = 8.0 \pm 3.1$ defined over the range of column densities from $\log(N_{\text{CaII}}/\text{cm}^{-2}) = 11.6$ to $\log(N_{\text{CaII}}/\text{cm}^{-2}) = 12.5$. The vertical solid line indicates the UVES 4σ detection limit $\log(N_{\text{CaII}}/\text{cm}^{-2}) = 10.7$ for the median S/N_r and the dotted line represents the maximal detection limit $\log(N_{\text{CaII}}^{\text{max}}/\text{cm}^{-2}) = 11.7$ for the minimal S/N_r . The minimal detection limit $\log(N_{\text{CaII}}^{\text{min}}/\text{cm}^{-2}) = 10.4$ for the maximal S/N_r is not plotted in this figure. The vertical errorbars are Poisson errors.

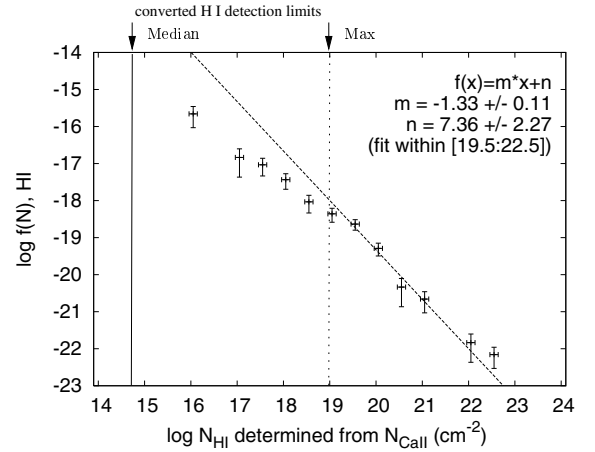


Fig. 3. The column density distribution function $f(N)$. The HI column densities are calculated from the Ca II column densities detected with UVES with the help of the correlation between the abundance $A(\text{Ca II})$ and N_{HI} (Wakker & Mathis 2000). The dashed line represents a power law fit $f(N) = CN^\beta$ with $\beta = -1.3 \pm 0.1$ and $\log C = 7.4 \pm 2.3$ defined over the range of column densities from $\log(N_{\text{HI}}/\text{cm}^{-2}) = 19.5$ to $\log(N_{\text{HI}}/\text{cm}^{-2}) = 22.5$. The vertical and horizontal errorbars indicate Poisson and statistical (from Voigt profile fitting) errors, respectively. The vertical solid and dotted lines indicate the converted 4σ median and maximal UVES detection limit.

to $\log(N_{\text{HI}}/\text{cm}^{-2}) = 22.5$. Figure 4 shows $f(N)$ for HI observed with Effelsberg in the same directions where we find Ca II/Na I absorption lines with UVES. The dashed line

represents a power law fit with $N_{\text{Eff}}^{-0.4}$ defined over the range of column densities from $\log(N_{\text{HI}}/\text{cm}^{-2}) = 18.5$ to $\log(N_{\text{HI}}/\text{cm}^{-2}) = 20$. Note, that we have only 14 absorption

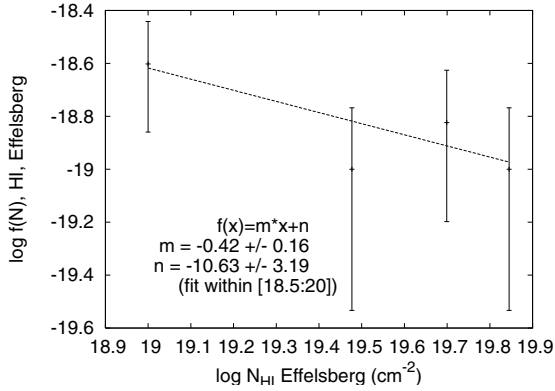


Fig. 4. The HI column density distribution observed with Effelsberg. The dashed line represents a power law fit over the range of column densities ($\log(N_{\text{HI}}/\text{cm}^{-2})$) from 18.5 to 20. The vertical errorbars indicate Poisson errors.

features along 13 lines of sight through the Galactic halo observed with the Effelsberg telescope. Therefore, the significance of the fit result is very poor. Furthermore, there is a bias in the Effelsberg data, because we only observed sight lines where Ca II absorption was detected.

Apparently, the slopes for the two different data sets deviate from each other. The most likely reason for this difference is that the above-used Ca II-to-HI column density conversion indeed is not appropriate for our absorbers because of the substantial uncertainties regarding ionisation, dust depletion and beam smearing effects. Note that the slope of our HI column density distribution (Fig. 3) shows a slight flattening at low column densities ($\log(N_{\text{HI}}/\text{cm}^{-2}) < 19$). This is most likely due to incompleteness caused by the detection limit of the UVES instrument. Another reason for the change in slope at small column densities could be the fact that we take both IVC and HVC gas as one sample into account for the statistical investigation. By using the correlation between $A(\text{Ca II})$ and N_{HI} (Wakker & Mathis 2000) we implicitly assume that IVCs and HVCs have the same intrinsic calcium abundance and similar dust-depletion properties, which is unrealistic because both populations probably have different origins (Galactic versus extragalactic; see Richter 2006, for a review). We will be able to discuss these effects in more detail when we have a larger sample of Ca II absorbers, so that we can separate intermediate- and high-velocity Ca II absorbers and treat them as different samples to get adequate statistical results for both populations.

4.2. Deviation velocities

Figure 5 shows the deviation velocity (Wakker 1991) of all observed intermediate- and high-velocity absorbers versus galactic longitude and latitude. The size of the triangles in Fig. 5 is proportional to the Ca II column densities observed with UVES. Obviously, there is no systematic trend in the velocity distribution. Note that we have no Ca II/Na I UVES data for the region $b > 0^\circ$ and $l < 200^\circ$. Therefore, our v_{dev} distribution is incomplete. This fact also becomes apparent in Fig. 1. We expect additional HST/STIS and KECK data for Ca II, Na I and other species to cover this region of the sky (Richter et al. 2008, in preparation).

Figure 6 shows the number of sight lines with intermediate or high velocity Ca II/Na I absorption lines plotted against deviation velocity. There is an accumulation at low deviation

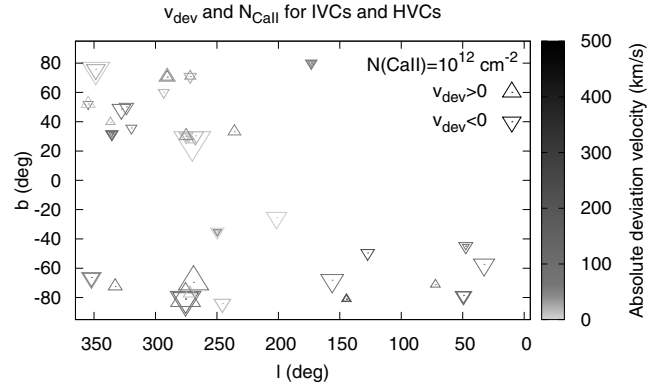


Fig. 5. Distribution of deviation velocities of the observed intermediate- and high-velocity absorbing systems versus galactic longitude and latitude. The dimensions of the triangles are proportional to the Ca II column densities observed with the UVES instrument. In the upper right corner of the diagram an exemplary Ca II column density of $N_{\text{CaII}} = 1 \times 10^{12} \text{ cm}^{-2}$ is shown.

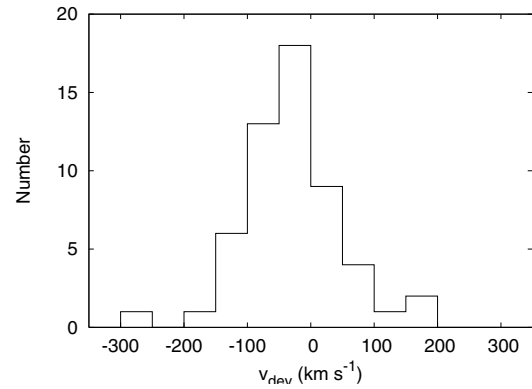


Fig. 6. Number of sight lines with intermediate- or high-velocity Ca II absorption lines versus deviation velocity.

velocities ($|v_{\text{dev}}| < 100 \text{ km s}^{-1}$). In addition, there appears to be a slight excess at negative v_{dev} . It is unlikely that this is due to a selection effect caused by our inhomogeneous all-sky sample. In the missing northern part of the sky most of the HVCs have negative LSR velocities due to the Galactic rotation. Therefore we also expect negative deviation velocities for this region of the sky. The slight excess for negative v_{dev} in our dataset is most likely due to systematic effects in connection with homogeneous structures infalling onto the Galactic disk.

Note that there is one sight line (QSO J0103+1316) with a very high deviation velocity of about $v_{\text{dev}} \approx -260 \text{ km s}^{-1}$. This sight line passes the region between the Anti-Centre Complex and the Magellanic Stream, where high negative LSR velocities are widely observed.

We also have searched for a possible correlation between the Ca II column densities and the deviation velocities. However, no such correlation is visible at this point. With 150 additional sight lines being available soon, we will be able to improve our statistical results.

4.3. Doppler b -parameters and component structure

Figure 7 shows the distribution of Doppler-parameters (b -values) for the intermediate or high velocity Ca II absorbers. The dashed vertical line indicates the UVES velocity resolution of $\Delta v_{\text{UVES}} \approx 7 \text{ km s}^{-1}$. Therefore, lines with $b < 7 \text{ km s}^{-1}$ are not resolved

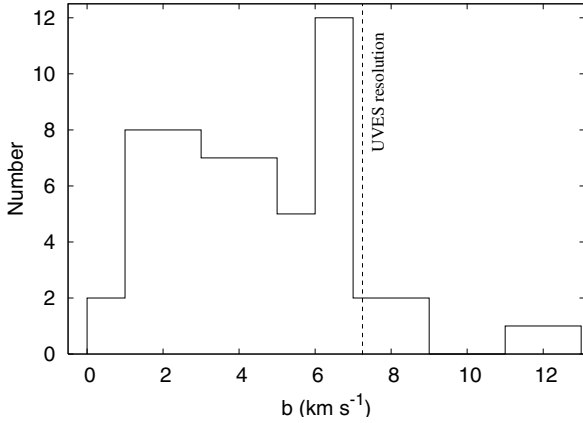


Fig. 7. Number of intermediate- and high-velocity Ca II absorption lines versus Doppler-parameter (b -value). The dashed vertical line indicates the UVES velocity resolution of $\Delta v_{\text{UVES}} \approx 7 \text{ km s}^{-1}$.

with the UVES instrument. However, the histogram indicates that the bulk of the Ca II lines have b values smaller than 7 km s^{-1} , and only a small fraction has $b > 7 \text{ km s}^{-1}$ (as securely obtained by the simultaneous fit of the two Ca II lines that have different f values). We can derive an upper temperature limit if we assume that the line width is dominated by thermal Doppler broadening.

$$T < \frac{b_{\text{therm}}^2 A}{f} \quad (7)$$

In this expression b is the Doppler parameter, A is the atomic weight and $f = 2 \times 10^{-6} \cdot k/u$ with k the Boltzmann constant and u the atomic mass unit. Assuming pure thermal line broadening a b -value of 7 km s^{-1} and $A_{\text{CaII}} = 40$ corresponds to a temperature of $T \approx 1.2 \times 10^5 \text{ K}$.

Since Ca II absorption traces mostly neutral gas, it is clear, however, that the b -value is dominated by turbulent gas motions rather than by the temperature of the gas. This is shown also by the much lower temperatures estimates from the measured 21 cm line widths (see Sect. 3). The fact that the bulk of the Ca II lines have b values of $< 7 \text{ km s}^{-1}$ indicates that turbulence and bulk motions in the gas are relatively small, suggesting that the absorbers are spatially confined in relatively small clumps on pc-scales. Sembach et al. (2003b) used FUSE data to study highly ionised (O VI) high-velocity absorbing systems along sight lines through the Galactic halo in the directions of 100 extragalactic objects. Compared to our absorbers these highly ionised systems have much higher b -values in the range of $16 \dots 72 \text{ km s}^{-1}$, suggesting that high-ion absorbers live in much more extended regions (kpc-scales) than the Ca II absorbers.

Systems that show Na I absorption possibly are even more confined, as the presence of Na I requires relatively high gas densities ($n_{\text{H}} > 0.1 \text{ cm}^{-3}$) to achieve a detectable level of neutral sodium, which has an ionisation potential of $< 10 \text{ eV}$. For a constant thermal gas pressure, on the other hand, high densities imply low temperatures of the gas.

This idea is supported by high-resolution ($R \sim 68\,000$) observations by Sembach et al. (1993) and Sembach & Danks (1994). They obtained a sample of spectra in the direction of 55 stars at distances above 2 kpc, containing 231 Na I and 312 Ca II components. 10% of the total Ca II column densities were found at forbidden velocities, while in case of Na I this is true only for a small fraction of few percent. The absorbers show a two-component temperature distribution of cold ($\sim 100 \text{ K}$) and

Table 3. Number of IVC/HVC Ca II absorption components observed with UVES and their absolute and percental values. The total number of sight lines which show Ca II absorption lines is 31. The last two columns show the data analysed by Prochter et al. (2006) for comparison. Their total number of sight lines is 25.

Number of components	Sight lines with Ca II absorption	[%]	Sight lines with Mg II absorption	[%]
1	17	55	5	20
2	7	23	13	52
3	4	13	2	8
4	3	1	3	12
5	0	0	1	4
6	0	0	0	0
7	0	0	1	4

warm (~ 1000 to 5000 K) gas in diffuse clouds and intercloud medium. Ca II traces both media, while Na I was detected preferentially in the cloudy medium.

Note that the presence of relatively cold, sub-pc and AU-scale structures in the Galactic halo gas has been proven by other observations. One sight line in the direction of PKS 1448–232 with distinct Ca II/Na I absorption and corresponding H I emission lines was recently observed by Richter et al. (2005) with the VLA. At an angular resolution of about $2'$ HPBW they detected several cold ($T < 1000 \text{ K}$) clumps of neutral gas with fairly low peak column densities of $N_{\text{HI}} \approx 7 \times 10^{18} \text{ cm}^{-2}$. In addition, ultraviolet measurements of molecular hydrogen in Galactic extraplanar clouds have shown that small, dense gaseous clumps at sub-pc scale are widespread in the lower halo, in particular in the intermediate-velocity clouds (Richter et al. 1999, 2003a,b).

To check whether a single or a multi-component absorption structure is typical for the extraplanar Ca II absorbers we have created a table containing the number of IVC/HVC Ca II absorption components (Table 3). Obviously, absorption systems with a single or a double absorption-component structure are more common (77%) than systems with more than two absorption components (16%).

5. Discussion of physical properties and origin of the absorbers

The fact that among 103 random lines of sight through the halo we observe 35 optical extraplanar absorption systems with at least one intermediate- or high-velocity component shows that the Milky Way halo contains a large number of neutral gas structures that give rise to intermediate- and high-velocity Ca II and Na I absorption.

5.1. Area filling factors

In the following we want to determine the area filling factors of our absorbers observed with UVES and Effelsberg. The area filling factor which we define is the fraction of sight lines which show Ca II absorption or H I absorption to the total number of observed sight lines. We get a total Ca II area filling factor of about 30% and a significantly larger H I area filling factor for the Effelsberg data of about 68%. Both factors are defined for the same lower H I column density regime as described above. The discrepancy between the total absorption and emission area filling factors could possibly be explained by the effect that the neutral gas structures that give rise to the Ca II absorption only

partly fill the $9'$ beam of the Effelsberg telescope. This could be an indication that the angular extent of the absorbers is small. The beam sizes of the different instruments (UVES, Effelsberg, LAB) also must have an effect on the column density distributions. Especially possible small-scale, high column density structures get affected by beam smearing, leading to a bias towards smaller column densities. The slope of the column-density distribution from 21 cm data therefore is expected to steepen with stronger beam-smearing. Thus, the different slopes of the HI column-density distributions from the UVES data and the Effelsberg data can be explained naturally by the limited beam size of the radio observations.

We also determined the area filling factor for our intermediate- and high-velocity Ca II absorbers separately. We distinguish between IVCs and HVCs by using the deviation velocity of the clouds as a separation criterion (see Sect. 4.2). The Ca II area filling factor is about 16% for the intermediate-velocity and about 17% for the high-velocity gas for converted HI column densities above $\log(N_{\text{HI}}/\text{cm}^{-2}) \approx 16$. Using our Effelsberg observations, we calculate an HI area filling factor of about 37% (IVCs) and 16% (HVCs) for densities above $\log(N_{\text{HI}}/\text{cm}^{-2}) \approx 18$.

The analysed UVES and Effelsberg spectra show that for several cases the Ca II and Na I absorbers have no intermediate- or high-velocity counterpart in the 21 cm data obtained with Effelsberg. This implies that the HI column densities of the Ca II and Na I absorption components at these velocities fall below the detection limit of the Effelsberg 21 cm observations and also of current large surveys like the LAB survey. Another possibility for this non-detection is a small diameter of the clouds, so that beam-smearing effects will again become important.

5.2. Possible association with known IVC or HVC complexes

The directions of 19 of the intermediate- and high-velocity clouds as well as their velocities indicate a possible association with known large and extended IVC or HVC complexes (Tables 1 and 2). Since we do not know the distances to the several absorbing systems the only criteria for the determination of a possible association with IVC/HVC complexes are the positions and the velocities.

Eight absorbing systems, and therefore the majority, are associated with the extensive Magellanic Stream (MS). In all eight cases the sight lines pass only the outer regions of the MS. In the case of QSO J0139–0824 and QSO J0105–1846 it is not clear if they are possibly parts of the MS or the Anti-Center shell (AC shell) because they are located in the intermediate range. Only for the sight line towards QSO J0003–2323 we have corresponding HI observations obtained with the 100-m telescope at Effelsberg.

Four systems are most likely associated with the intermediate-velocity Spur (IV-Spur). The sight lines toward QSO J1211+1030 and QSO B1331+170 pass the inner, denser part of the IV-Spur whereas the sight lines in the direction of QSO B0952+179 and QSO B2314–409 are located in the outer, clumpy structures of the complex. For three of these sight lines we have additional HI observations but only in one case (QSO J1211+1030) we found a corresponding emission line.

The position and the velocity of the absorbing systems in the direction of QSO B1212+3326 indicate that these systems are possibly part of the inner region of the intermediate-velocity Arch (IV-Arch). For these sight line we have obtained additional HI data. Only one component has a counterpart in HI.

One absorption component in the direction of QSO J1039–2719 is most likely associated with the HVC complex WD. We re-observed this sight line with the 100-m telescope at Effelsberg but we find no corresponding HI emission lines.

The sight line towards QSO B0458–0203 passes the very outer regions of the Anti-Center shell. The HI data reveal a corresponding emission line.

The velocity and the coordinates of the absorption component with the high positive LSR velocity in the direction of QSO B1101–26 is possibly associated with the Leading Arm (LA) of the Magellanic System. The sight line passes the outer region of the LA. The Effelsberg data show no corresponding HI emission line.

The absorbing systems towards QSO 1448–232 are possibly associated with the HVC complex L (Richter et al. 2005).

The two absorbing components in the direction of QSO J2155–0922 are possibly part of the HVC complex GCN. The Effelsberg data show no corresponding HI emission line.

5.3. Comparison with Mg II systems and column density distribution functions

It is evident that low-column density intermediate- and high-velocity Ca II absorbers have a large area filling factor because of the high Ca II and Na I detection rate. If these absorbers represent a typical phenomenon of spiral galaxies like our Milky Way or M 31 and if they are located in the halo of these galaxies, they should produce HI Lyman-Limit and Mg II absorption along sight lines which pass through the halo gas of other galaxies. There are two different populations of Mg II absorbers, the weak ($W_{\lambda 2796} \leq 0.3 \text{ \AA}$) and the strong ($W_{\lambda 2796} > 0.3 \text{ \AA}$) Mg II systems. While the weak Mg II absorbers are thought to be located in the outskirts of galaxies (e.g., Churchill et al. 1999), the strong Mg II systems are most likely located in the halo (e.g., Petitjean & Bergeron 1990; Charlton & Churchill 1998; Ding et al. 2003b) or even in the discs of galaxies (Damped Lyman Alpha systems, DLAs, Rao et al. 2006), and they possibly represent the analogues of IVCs/HVCs (e.g., Savage et al. 2000). In fact, many of the properties of the high-velocity Ca II and Na I absorption lines resemble those of the strong Mg II absorption line systems observed in the circumgalactic environment of other galaxies (Ding et al. 2003a; Bouché et al. 2006; Prochter et al. 2006). The high-velocity Ca II and Na I absorbers thus may possibly represent the Galactic counterparts of strong Mg II systems at low redshift.

In Sect. 4 we have shown that absorption systems at intermediate and high velocities with a single or a double absorption component structure are more common than systems with more than two absorption components. The analysis of strong Mg II absorption systems by Prochter et al. (2006) shows that there is a tendency for two or more Mg II absorption lines (Table 3). The more complex absorption structure for Mg II systems can be explained by longer sight lines through the halo of the host galaxy compared to the typically shorter sight lines through the halo of the Milky Way. Our statistical analysis shows that there is no obvious difference in the observed parameters of single-component and multi-component absorption systems. As described by Ding et al. (2005), multiple cloud components in absorption systems can be divided into two sub-classes. The “kinematically spread” absorbers show one or more dominant Ca II absorbers and several weaker ones spread over a wide velocity range, as seen towards QSO 0109–3518 and QSO B1101–26 (Figs. 9 and 12, online version). The

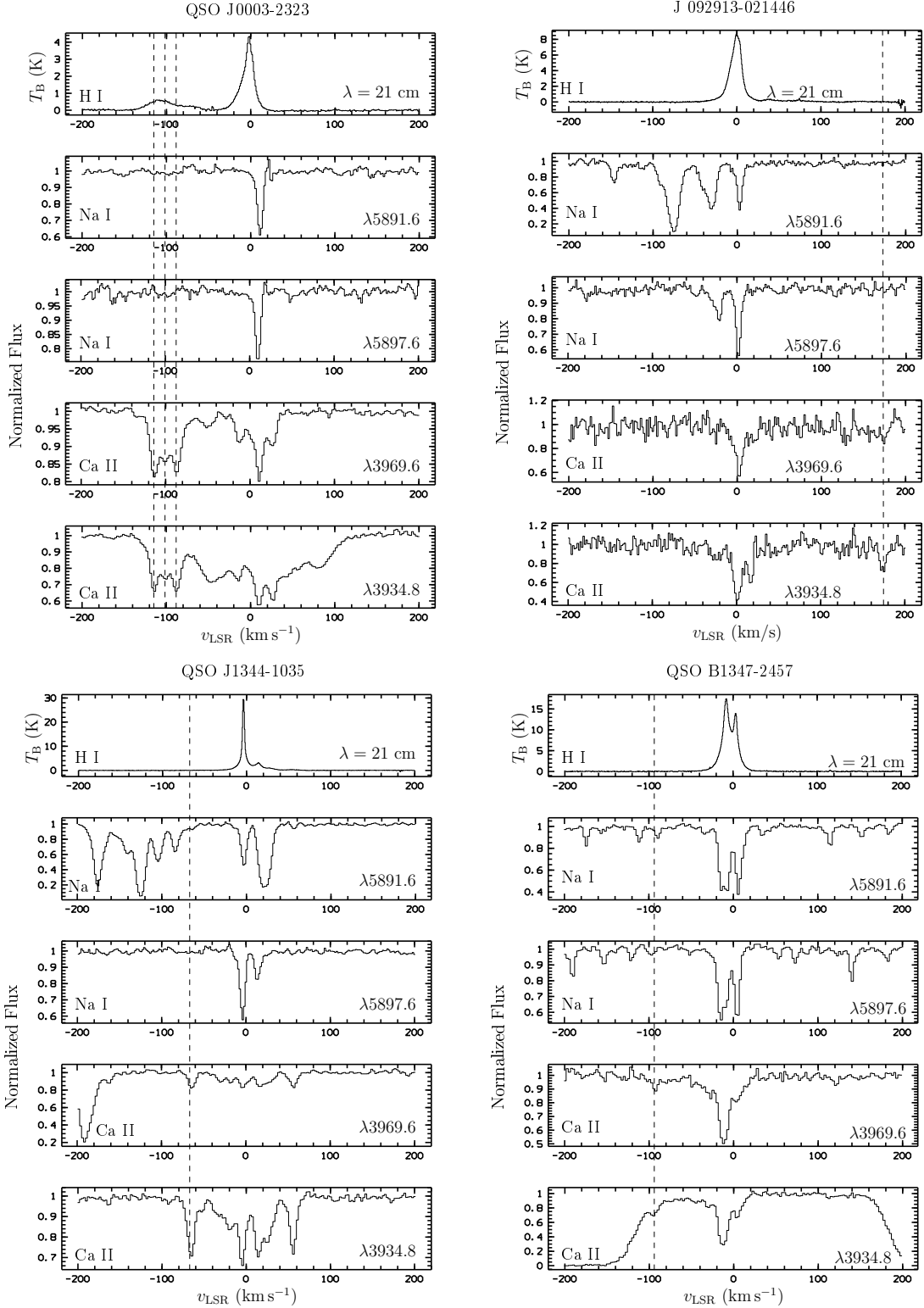


Fig. 8. Ca II and Na I absorption and H I emission spectra in the direction of the quasars QSO J0003–2323, J092913–021446, QSO J1344–1035, and QSO B1347–2457 obtained with UVES and the Effelsberg 100-m telescope, respectively. The absorption and corresponding emission lines are indicated by dashed lines.

“kinematically compact” subclass is characterised by multiple absorption components with comparable equivalent widths blended together and spread over less than about 100 km s⁻¹. An example of the latter sub-class is the absorber towards QSO J0003-2323, as displayed in Fig. 8.

Important information about the distribution of neutral and weakly ionised extraplanar gas in the Milky Way is provided by column density distribution functions $f(N)$ of Ca II and H I that we have derived in Sect. 4. We now can compare the properties of these distribution functions with results from QSO

absorption-line studies and extragalactic H I surveys. The slope of the Ca II column density distribution of Milky Way absorbers turns out to be $\beta = -1.6 \pm 0.3$. This is identical to the slope of $\beta = -1.59 \pm 0.05$ derived for strong Mg II absorbers at intermediate redshifts ($z = 0.4-1.2$), as presented by Churchill et al. (2003). The equality of the slopes suggests that (despite somewhat different ionisation and dust-depletion properties) Ca II and strong Mg II absorbers probe similar gaseous structures that are located in the environment of galaxies.

Concerning neutral hydrogen, Petitjean et al. (1993) have investigated the H I column density distribution function of intergalactic QSO absorption line systems at high redshift (mean redshift of $z \approx 2.8$) with the help of high spectral resolution data. Their H I data span a range from $\log(N_{\text{HI}}/\text{cm}^{-2}) = 12$ to $\log(N_{\text{HI}}/\text{cm}^{-2}) = 22$. After they could show that a single power law with a slope of $\beta = -1.49$ provides only a poor fit to the data they divided the sample into two subsamples (lower and higher than 10^{16} cm^{-2}). They found a slope of $\beta = -1.83$ for the $\log(N_{\text{HI}}/\text{cm}^{-2}) < 16$ sample and $\beta = -1.32$ for the $\log(N_{\text{HI}}/\text{cm}^{-2}) > 16$ sample. Petitjean et al. (1993) point out that the overall H I distribution is more complex than had been thought and that even two power laws only poorly fit the data. In a later study, Kim et al. (2002) indeed show that the slope of the H I column density distribution varies between ~ -1.4 and ~ -2.0 , depending on the mean absorber redshift and the column-density interval used. Unfortunately, very little is known about the H I absorber distribution in the for us interesting range $\log(N_{\text{HI}}/\text{cm}^{-2}) = 15 \dots 19$ and $z = 0 \dots 0.5$ due to the lack of low-redshift QSO data in the UV band.

Although we have substantial uncertainties in the conversion of Ca II into H I as discussed above, it is interesting that the slope of the H I column density distribution of $\beta = -1.3 \pm 0.1$, as indirectly derived from our Ca II data for the $\log(N_{\text{HI}}/\text{cm}^{-2})$ range between 19 and 22, is in general agreement with the statistics of low- and high-redshift QSO absorption line data. This implies that a significant fraction of high-column density ($\log N > 16$) intervening QSO absorbers are closely related to galaxies in a way similar as the intermediate- and high-velocity Ca II absorbers are connected to the Milky Way. It appears that the column density distribution of extraplanar neutral gas structures (i.e., HVCs and their extragalactic analogues) is roughly universal at low and high redshift. This underlines the Overall importance of the processes that lead to the circulation of neutral gas in the environment of galaxies (e.g., fountain flows, gas accretion, tidal interactions) for the evolution of galaxies.

6. Summary and outlook

We studied optical absorption of Ca II and Na I (archival VLT/UVES data) and H I 21 cm emission (Effelsberg telescope) in the direction of quasars. The major results of our project are:

1. intermediate- and high-velocity Ca II/Na I absorption is found along 35 out of 103 studied lines of sight in the direction of quasars. In total we found 55 individual absorption components;
2. in some cases the Ca II absorption lines are associated with known intermediate- and high-velocity clouds, but in other cases the observed absorption has no 21 cm counterpart;
3. The observed Ca II column density distribution follows a power-law $f(N) = CN^\beta$ with a slope of $\beta \approx -1.6$;
4. this distribution is similar to the distribution found for intervening Mg II systems that trace the gaseous environment of other galaxies at low and high redshift. After having

transformed the observed Ca II column densities into H I column densities we find that the extraplanar absorbers trace neutral gas structures with logarithmic H I column densities on the order of $\log(N_{\text{HI}}/\text{cm}^{-2}) \approx 18 \dots 20$;

5. the physical and statistical properties of the Ca II absorbers suggest that these structures represent the local counterparts of strong ($W_{\lambda 2796} > 0.3 \text{ \AA}$) Mg II absorbing systems that are frequently observed at low and high redshift in QSO spectra and that are believed to trace the environment of other galaxies;
6. most of the absorbers are characterised by single-component absorption with b values of $< 7 \text{ km s}^{-1}$.

For the future we are planning to extend our study of extraplanar Ca II absorbers using additional high-resolution data from UVES as well as KECK data. Using radio synthesis telescopes, we are further planning to re-observe several sight lines with Ca II/Na I absorption and H I emission. These high-resolution observations are crucial to search for related small-scale H I structures that are possibly not resolved with the Effelsberg telescope (see also Hoffman et al. 2004; Richter et al. 2005). Finally, we are currently analysing several ultraviolet QSO spectra from HST/STIS to measure weak metal line absorption in the Milky Way halo (in particular, absorption from neutral and weakly ionised species such as O I, Si II, and others). This will allow us to determine metallicities of the low-column density gas in the Milky Way halo. Metal abundance is an important parameter that will help to clarify whether the extraplanar gaseous structures are of Galactic or extragalactic origin. Furthermore, the high-resolution H I data in combination with the VLT/UVES and STIS data will enable us to study the physical parameters of these low column density gaseous structures, such as temperature and density, to better understand the connection between the different gas phases in the Milky Way halo. As mentioned before, the properties of the Ca II and Na I absorption lines resemble those of the Mg II absorption line systems observed in the environment of other galaxies. Studying the Galactic halo with the proposed strategy thus will provide important new insights into absorption line systems that are commonly observed in the halos of more distant galaxies.

Acknowledgements. Thanks to Benjamin Winkel and Peter Ernie for their helping hands. N.B.B. and P.R. acknowledge support by the DFG through DFG Emmy-Noether grant Ri 1124/3-1. T.W. was supported by the DFG through grant KE 757/4-2. Based on observations with the 100-m telescope of the MPIfR (Max-Planck-Institut für Radioastronomie) at Effelsberg.

References

- Adams, W. S. 1949, ApJ, 109, 354
 Arnal, E. M., Bajaja, E., Larrarte, J. J., Morras, R., & Pöppel, W. G. L. 2000, A&AS, 142, 35
 Bajaja, E., Arnal, E. M., Larrarte, J. J., et al. 2005, A&A, 440, 767
 Bergeron, J., Petitjean, P., Aracil, B., et al. 2004, The Messenger, 118, 40
 Bouché, N., Murphy, M. T., Péroux, C., Csabai, I., & Wild, V. 2006, MNRAS, 813
 Braun, R., & Burton, W. B. 1999, A&A, 341, 437
 Bregman, J. N. 1980, ApJ, 236, 577
 Charlton, J. C., & Churchill, C. W. 1998, ApJ, 499, 181
 Charlton, J. C., Churchill, C. W., & Rigby, J. R. 2000, ApJ, 544, 702
 Churchill, C. W., Rigby, J. R., Charlton, J. C., & Vogt, S. S. 1999, ApJS, 120, 51
 Churchill, C. W., Vogt, S. S., & Charlton, J. C. 2003, AJ, 125, 98
 de Heij, V., Braun, R., & Burton, W. B. 2002, A&A, 391, 159
 Dekker, H., D’Odorico, S., Kaufer, A., Delabre, B., & Kotzlowski, H. 2000, in Optical and IR Telescope Instrumentation and Detectors, ed. M. Iye, & A. F. Moorwood, Proc. SPIE, 4008, 534
 Ding, J., Charlton, J. C., Bond, N. A., Zonak, S. G., & Churchill, C. W. 2003a, ApJ, 587, 551
 Ding, J., Charlton, J. C., Churchill, C. W., & Palma, C. 2003b, ApJ, 590, 746

- Ding, J., Charlton, J. C., & Churchill, C. W. 2005, *ApJ*, 621, 615
- Fraternali, F. & Binney, J. J. 2006, *MNRAS*, 366, 449
- Fraternali, F., Binney, J., Oosterloo, T., & Sancisi, R. 2007, *New Astron. Rev.*, 51, 95
- Hartmann, D., & Burton, W. B. 1997, *Atlas of Galactic Neutral Hydrogen* (Cambridge, UK: Cambridge University Press), ed. D. Hartmann, & W. B. Burton, 243
- Hoffman, G. L., Salpeter, E. E., & Hirani, A. 2004, *AJ*, 128, 2932
- Kalberla, P. M. W. 2003, *ApJ*, 588, 805
- Kalberla, P. M. W., Burton, W. B., Hartmann, D., et al. 2005, *A&A*, 440, 775
- Kim, T.-S., Carswell, R. F., Cristiani, S., D'Odorico, S., & Giallongo, E. 2002, *MNRAS*, 335, 555
- Majewski, S. 2004, in *Satellites and Tidal Streams*, ed. F. Prada, D. Martinez Delgado, & T. J. Mahoney, *ASP Conf. Ser.*, 327, 63
- Masiero, J. R., Charlton, J. C., Ding, J., Churchill, C. W., & Kacprzak, G. 2005, *ApJ*, 623, 57
- Mathewson, D. S., Cleary, M. N., & Murray, J. D. 1974, *ApJ*, 190, 291
- Muller, C. A., Oort, J. H., & Raimond, E. 1963, *C. R. Acad. Sc. Paris*, 257, 1661
- Münch, G. 1952, *PASP*, 64, 312
- Petitjean, P., & Bergeron, J. 1990, *A&A*, 231, 309
- Petitjean, P., Webb, J. K., Rauch, M., Carswell, R. F., & Lanzetta, K. 1993, *MNRAS*, 262, 499
- Prochter, G. E., Prochaska, J. X., & Burles, S. M. 2006, *ApJ*, 639, 766
- Putman, M. E., de Heij, V., Staveley-Smith, L., et al. 2002, *AJ*, 123, 873
- Rao, S. M., Turnshek, D. A., & Nestor, D. B. 2006, *ApJ*, 636, 610
- Richter, P. 2006, in *Rev. Mod. Astron.* 19, ed. S. Roeser, 31
- Richter, P., de Boer, K. S., Widmann, H., et al. 1999, *Nature*, 402, 386
- Richter, P., Savage, B. D., Sembach, K. R., Tripp, T. M., & Jenkins, E. B. 2003a, in *The IGM/Galaxy Connection. The Distribution of Baryons at $z = 0$* , ed. J. L. Rosenberg, & M. E. Putman, *Ap&SS Library*, 281, 85
- Richter, P., Wakker, B. P., Savage, B. D., & Sembach, K. R. 2003b, *ApJ*, 586, 230
- Richter, P., Westmeier, T., & Brüns, C. 2005, *A&A*, 442, L49
- Savage, B. D., & Massa, D. 1987, *ApJ*, 314, 380
- Savage, B. D., Wakker, B., Jannuzi, B. T., et al. 2000, *ApJS*, 129, 563
- Sembach, K. R., & Danks, A. C. 1994, *A&A*, 289, 539
- Sembach, K. R., & Savage, B. D. 1996, *ApJ*, 457, 211
- Sembach, K. R., Savage, B. D., & Massa, D. 1991, *ApJ*, 372, 81
- Sembach, K. R., Danks, A. C., & Savage, B. D. 1993, *A&AS*, 100, 107
- Sembach, K. R., Wakker, B. P., Savage, B. D., et al. 2003a, *ApJS*, 146, 165
- Sembach, K. R., Wakker, B. P., Savage, B. D., et al. 2003b, *ApJS*, 146, 165
- Shapiro, P. R., & Benjamin, R. A. 1991, *PASP*, 103, 923
- Shapiro, P. R., & Field, G. B. 1976, *ApJ*, 205, 762
- Spitzer, L. J. 1956, *ApJ*, 124, 20
- Thom, C., Putman, M. E., Gibson, B. K., et al. 2006, *ApJ*, 638, L97
- van Woerden, H., Schwarz, U. J., Peletier, R. F., Wakker, B. P., & Kalberla, P. M. W. 1999, *Nature*, 400, 138
- Wakker, B. P. 1991, *A&A*, 250, 499
- Wakker, B. P. 2001, *ApJS*, 136, 463
- Wakker, B. P., & Mathis, J. S. 2000, *ApJ*, 544, L107
- Wakker, B. P., York, D. G., Howk, J. C., et al. 2007, *ApJ*, 670, L113
- Wakker, B. P., York, D. G., Wilhelm, R., et al. 2008, *ApJ*, 672, 298
- Westmeier, T. 2007, Ph.D. Thesis, Rheinische Friedrich-Wilhelms-Universität Bonn

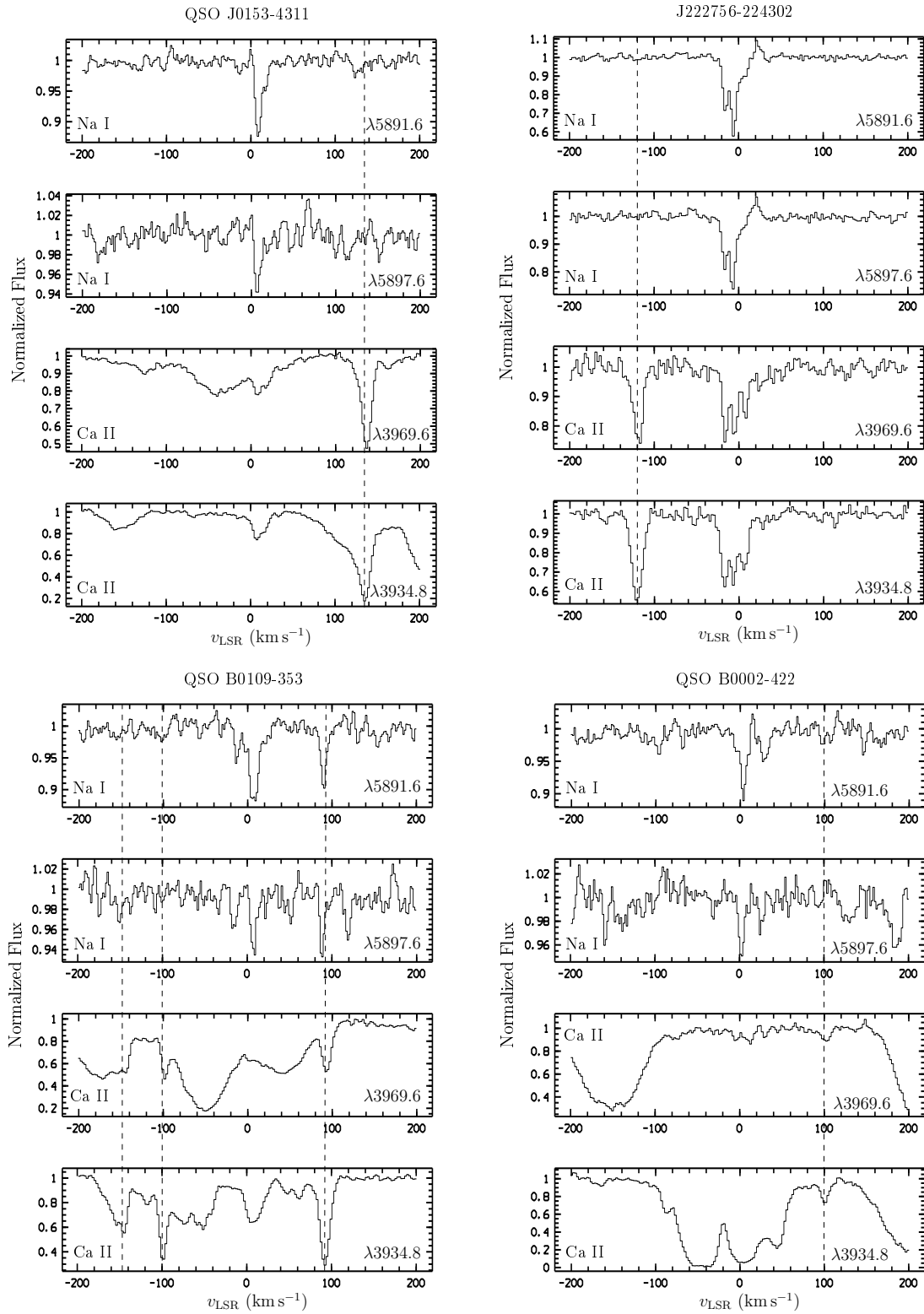


Fig. 9. Ca II and Na I absorption spectra of QSO J0153–4311, J222756–224302, QSO B0109–353, and QSO B0002–422 obtained with UVES. For these sight lines no Effelsberg data are available.

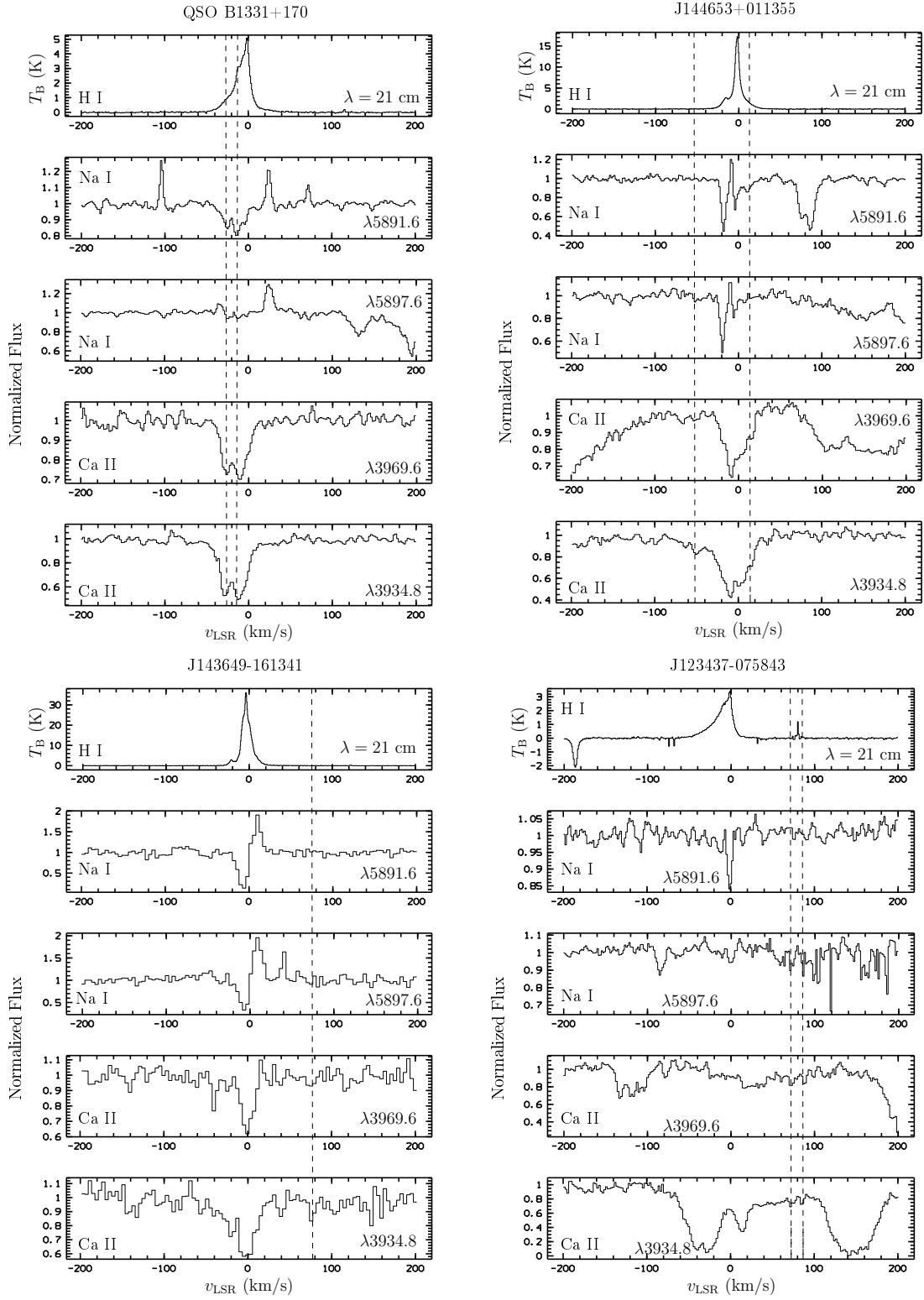


Fig. 10. Ca II and Na I absorption spectra of QSO B1331+170+2411 J144653+011355, J143649-161341, and J123437-075843 obtained with UVES. Additionally the corresponding H I emission line profiles measured with the Effelsberg 100-m telescope are shown. The spikes in the Effelsberg spectra of J123437-075843 are radio frequency interferences (RFI).

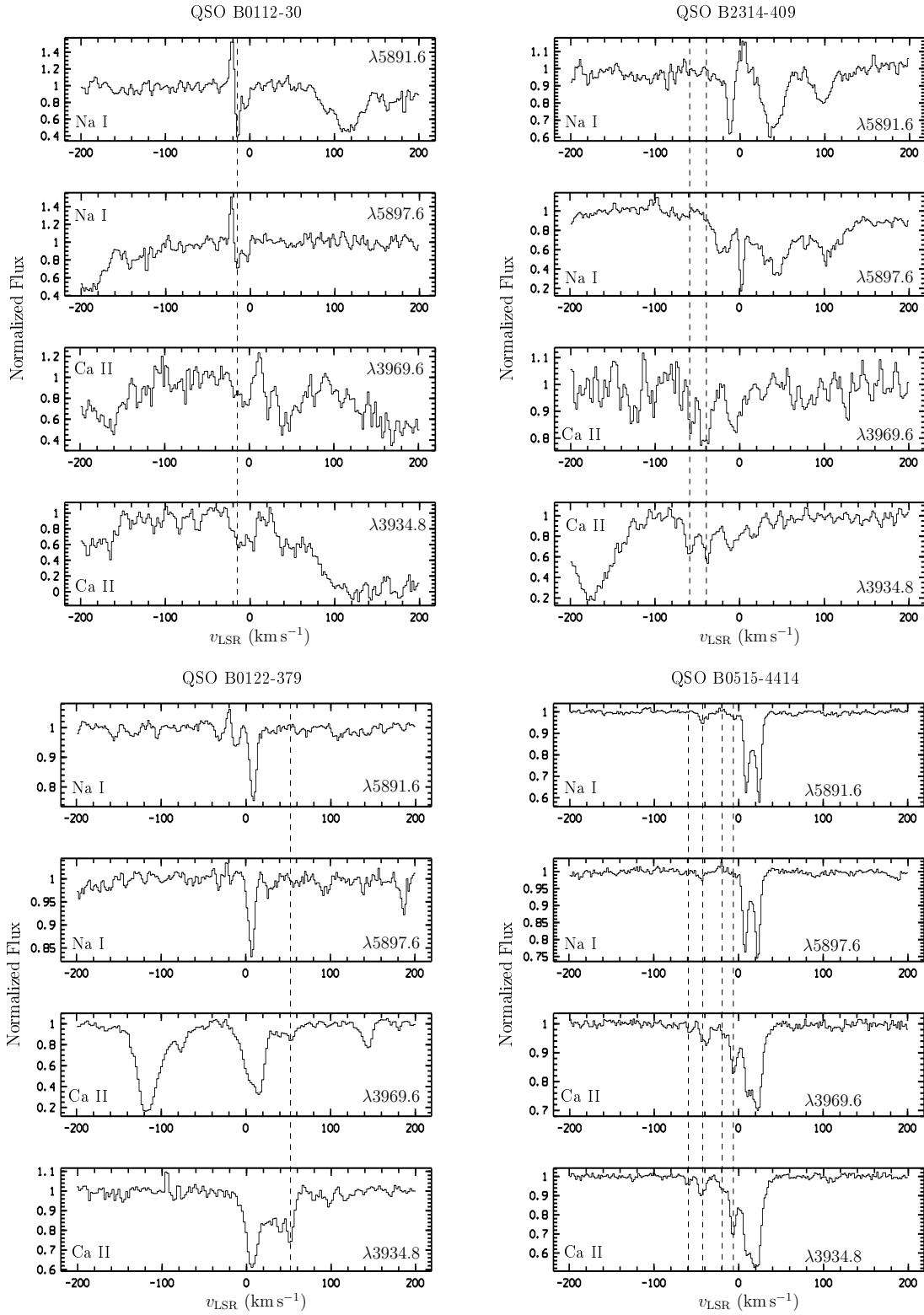


Fig. 11. Ca II and Na I absorption spectra of QSO B0112–30, QSO B2314–409, QSO B0122–379, and QSO B0515–4414 obtained with UVES. For these sight lines no Effelsberg data are available.

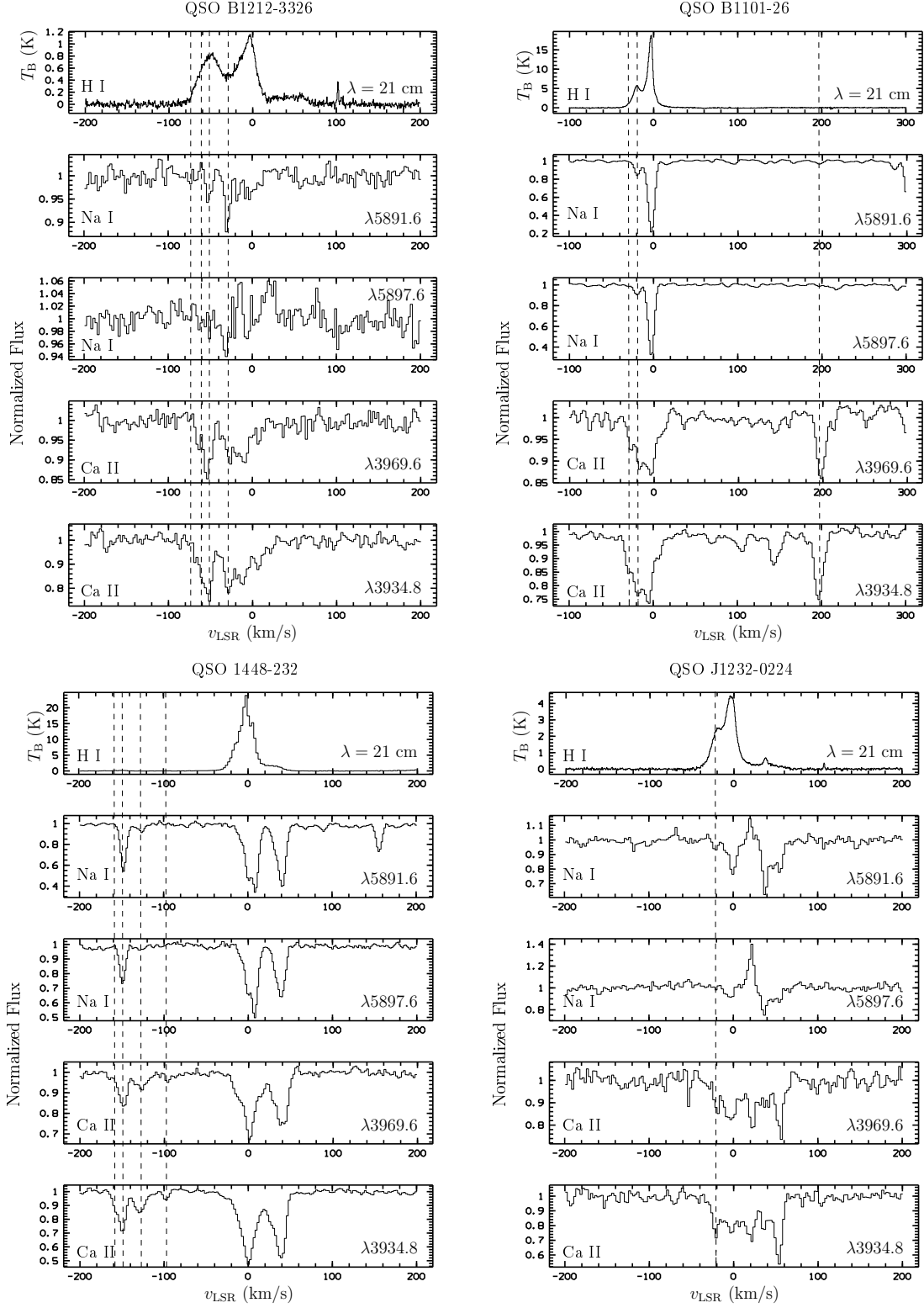


Fig. 12. Ca II and Na I absorption and corresponding H I emission spectra of QSO B1212+3326, QSO B1101–26, QSO 1448–232, and QSO J1232-0224 obtained with UVES and the Effelsberg 100-m telescope, respectively.

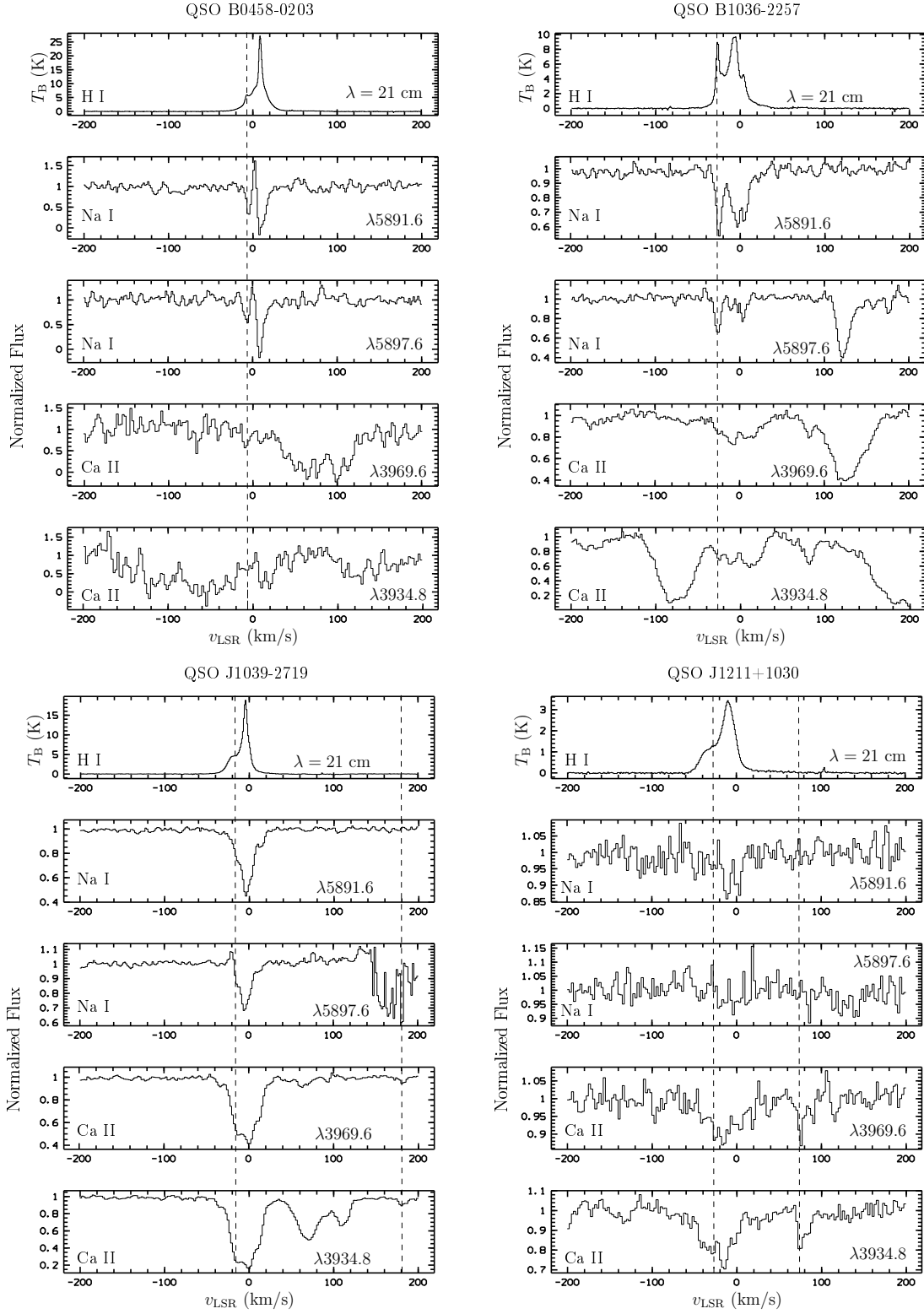


Fig. 13. Ca II and Na I absorption spectra of QSO B0458–0203, QSO B1036–2257, QSO J1039–2719, and QSO J1211+1030 obtained with UVES. Additionally the corresponding H I emission line profiles measured with the Effelsberg 100-m telescope are shown.

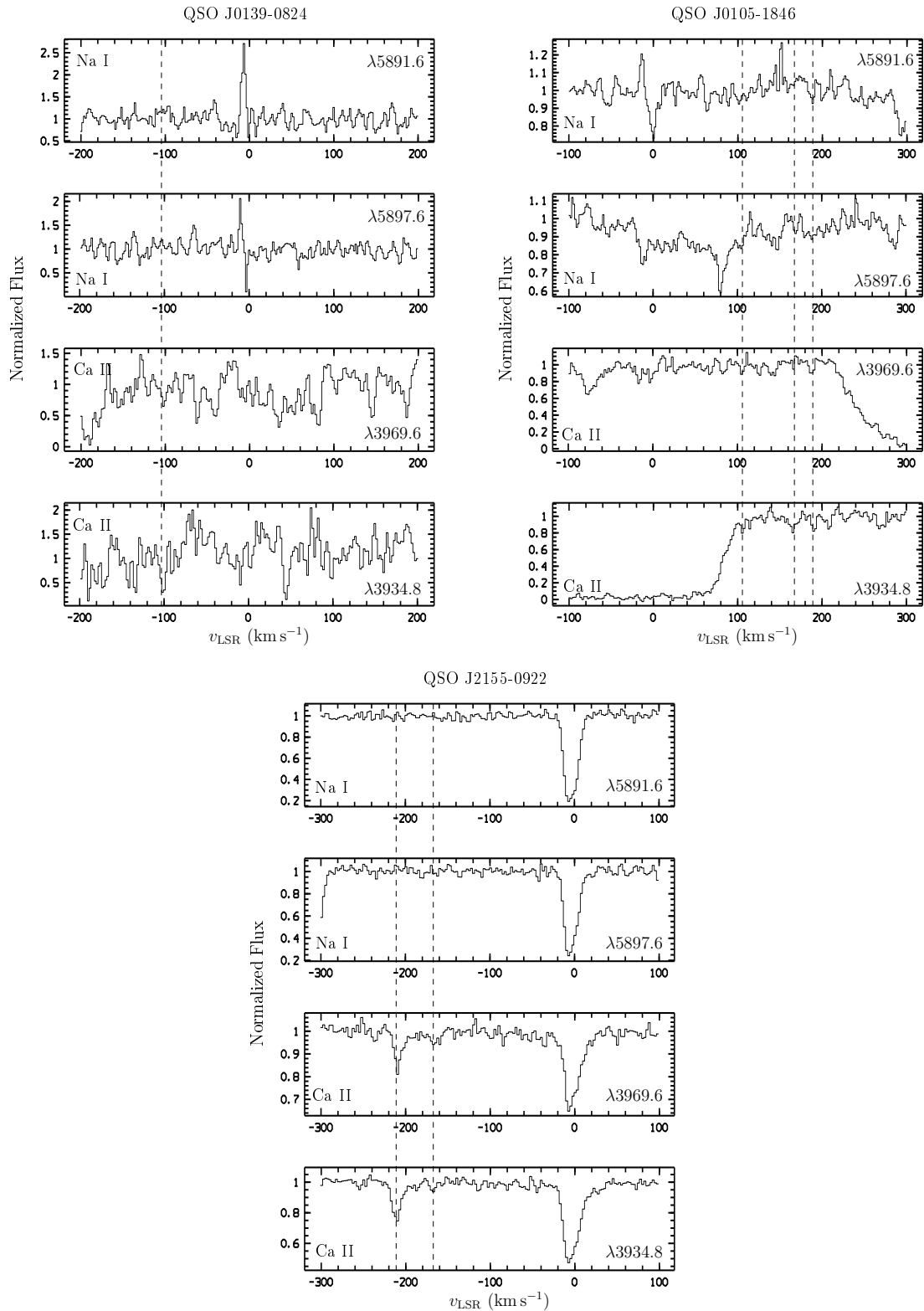


Fig. 14. Ca II and Na I absorption spectra of QSO J0139–0824, QSO J0105–1846, and QSO J2155–0922 obtained with UVES. No Effelsberg data are available.

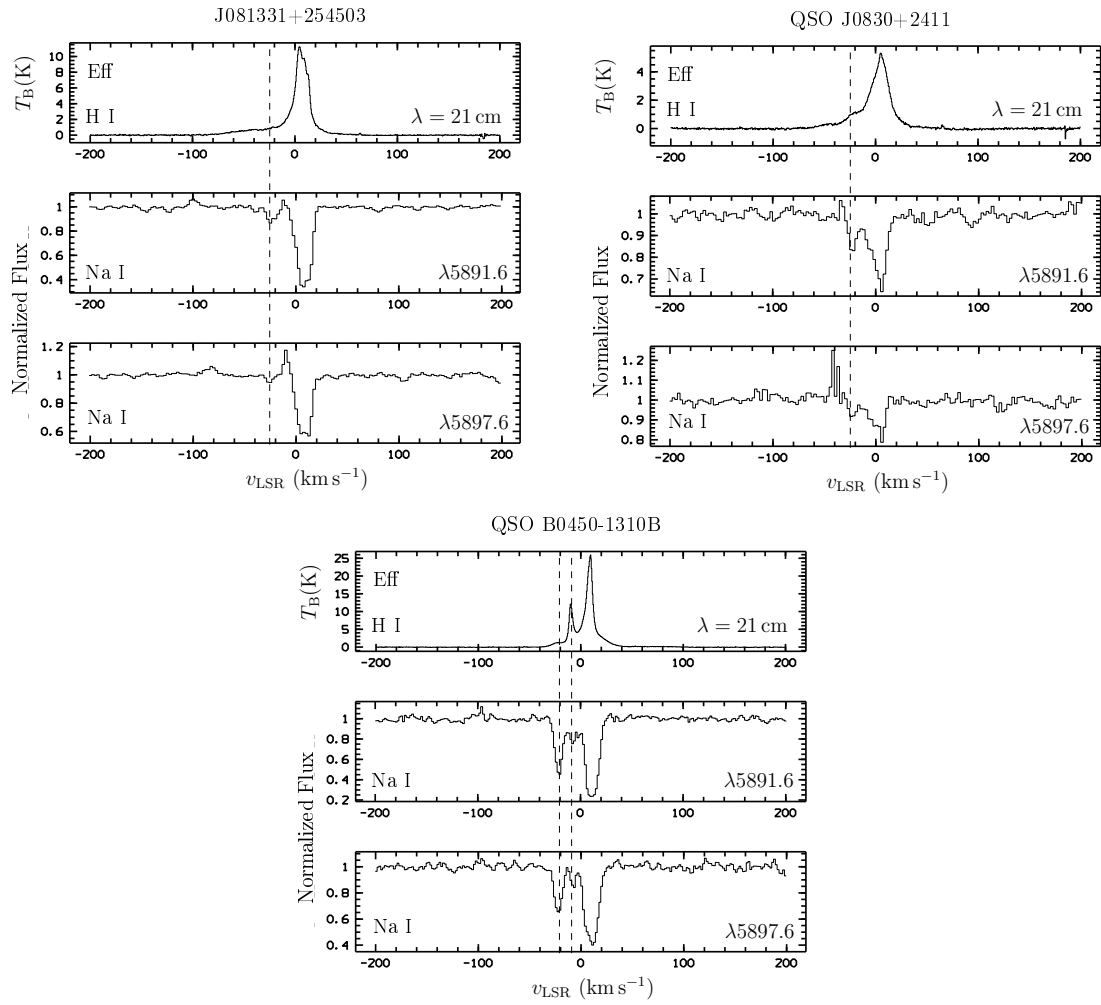


Fig. 15. Na I absorption and H I emission spectra in the direction of the quasars J081331+254503, QSO J0830+2411, and QSO B0450-1310B obtained with UVES and the Effelsberg 100-m telescope. For these sight lines no Ca II data are available.

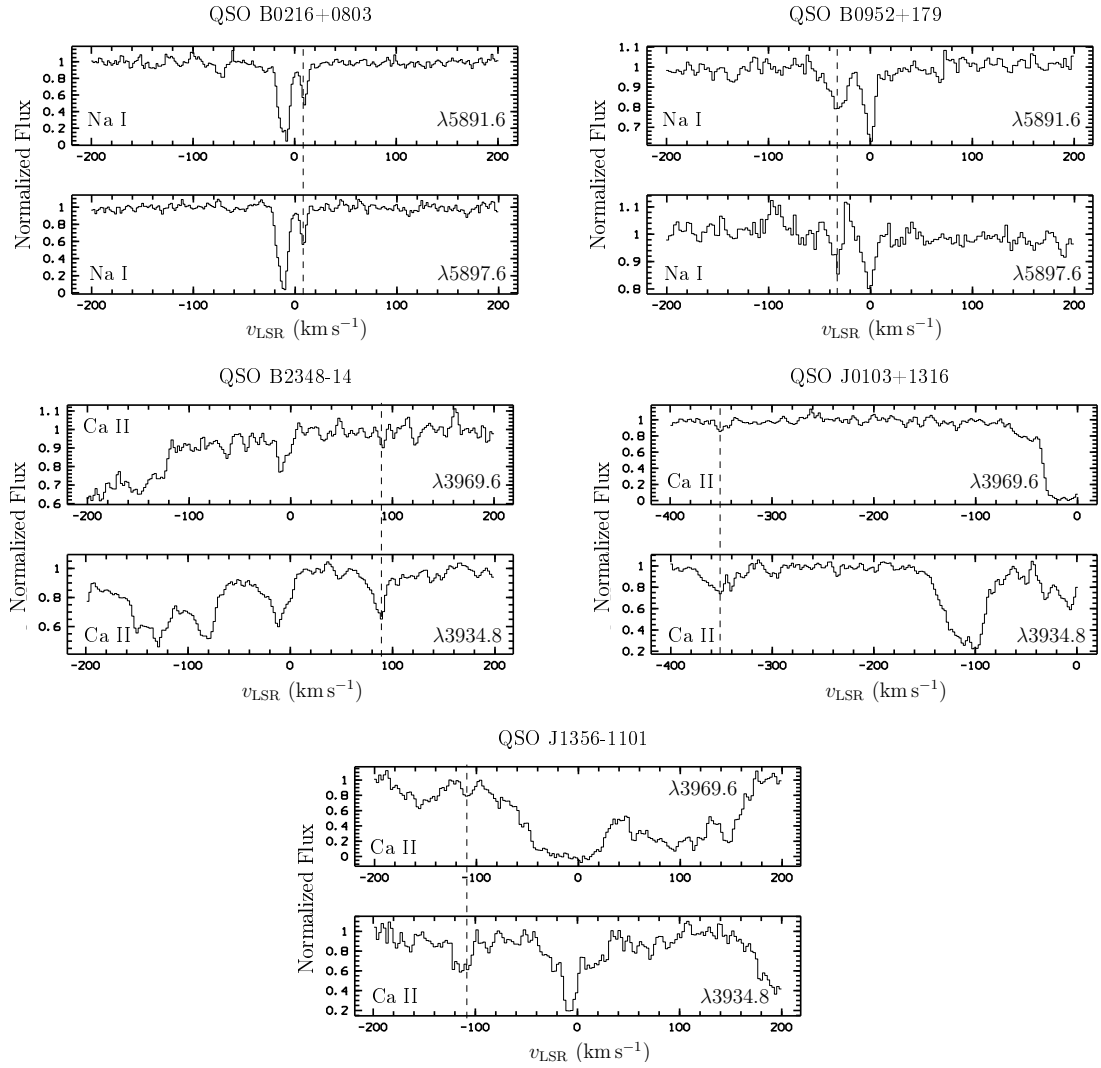


Fig. 16. *Upper row:* Na I absorption spectra of QSO B0216+0803 and QSO B0952+179 obtained with UVES. There are no Ca II data available. *Middle and lower rows:* Ca II absorption spectra of QSO B2348-147, QSO J0103+1316, and QSO J1356-1101 obtained with UVES. There are no Na I data available. For all five sight lines we have no Effelsberg data.